



Published in final edited form as:

IEEE Trans Ultrason Ferroelectr Freq Control. 2005 April ; 52(4): 672–681.

Design and fabrication of a 40-MHz annular array transducer

Jeffrey A. Ketterling and Frederic L. Lizzi

J. A. Ketterling and F. L. Lizzi are with Riverside Research Institute, New York, NY (email:ketterling@rrinyc.org).

Orlando Aristizábal and Daniel H. Turnbull

O. Aristizábal and D. H. Turnbull are with Skirball Institute of Biomolecular Medicine and New York University School of Medicine, New York, NY.

Abstract

This paper investigates the feasibility of fabricating a 5-ring, focused annular array transducer operating at 40 MHz. The active piezoelectric material of the transducer was a 9- μm thick polyvinylidene fluoride (PVDF) film. One side of the PVDF was metallized with gold and forms the ground plane of the transducer. The array pattern of the transducer and electrical traces to each annulus were formed on a copper-clad polyimide film. The PVDF and polyimide were bonded with a thin layer of epoxy, pressed into a spherically curved shape, and then back filled with epoxy. A 5-ring transducer with equal area elements and 100 μm kerfs between annuli was fabricated and tested. The transducer had a total aperture of 6 mm and a geometric focus of 12 mm. The pulse/echo response from a quartz plate located at the geometric focus, two-way insertion loss (IL), complex impedance, electrical cross-talk, and lateral beamwidth were all measured for each annulus. The complex impedance data from each element were used to perform electrical matching and the measurements were repeated. After impedance matching, $f_c \approx 36$ MHz and BWs ranged from 31 to 39%. The ILs for the matched annuli ranged from -28 to -38 dB.

I. INTRODUCTION

The field of high-frequency ultrasound (HFU) imaging, using frequencies above 20 MHz, is growing rapidly as transducer technologies improve and the cost of high bandwidth electronic instrumentation decreases. There are two main advantages of HFU transducers. First, they have a large bandwidth which provides fine scale axial resolution. Second, they have a small lateral beamwidth which permits imaging with resolution on the order of a wavelength ($\lambda = 37 \mu\text{m}$ at 40 MHz). However, single element focused transducers, currently used for most HFU applications, also have a small depth of field, limiting the best image resolution to a small axial range close to the geometric focus of the transducer.

The earliest work with HFU transducers utilized single element focused transducers fabricated with PVDF membranes as their active acoustic layer [1], [2]. These transducers were relatively easy to fabricate but suffered from a fairly high two-way insertion loss (≈ 40 dB) because of the material properties of PVDF. This resulted in a focus on methods to improve the insertion loss by optimizing the drive electronics and electrical matching [3]-[7]. At the same time, methods of fabricating single element HFU transducers using ceramic material were also being refined, and numerous devices were fabricated successfully to operate in the HFU regime [8]-[10]. These devices have an inherent advantage over PVDF based transducers because of their much lower insertion loss. However, single element PVDF transducers continue to be the primary transducer choice for HFU applications. Both PVDF and ceramic transducers have

been used to great success for ophthalmic [11], [12], dermatological [13]-[15], and small animal imaging [16]-[18].

The current emphasis on HFU transducers is targeted more towards array technology. An array permits electronic focusing that both improves the depth of field of the device and permits a 2D image to be constructed without mechanically scanning the transducer. Technologies such as CMUT [19], MEMS [20], as well as more traditional ceramic materials are being pursued [21], [22]. These methods all aim to fabricate individual array elements on the order of $\lambda/2$; these small dimensions necessitate advances in interconnects and electronics to fully implement the technologies.

In the interim, a more practical approach is to develop annular arrays with element sizes similar to current single element transducers. The advantage of an annular array is that it permits an increased depth of field along a line focus with a relatively limited number of elements. The primary drawback is that it must be mechanically scanned to generate a 2D image. Both passively focused and unfocused annular arrays are now being pursued. Ceramic materials are typically used for flat arrays because they are difficult to grow or to press into curved shapes [23]-[25]. PVDF is more advantageous in this respect because it can be easily press fit into a curved shape. PVDF also provides a better acoustic impedance match to water and biological tissue. Alves et. al [26] were able to fabricate a PVDF annular array but did not generate images or fully implement the array's functionality.

Here, we demonstrate the feasibility of a new method to construct PVDF based annular arrays. The active acoustic element of the transducer is a 9 μm PVDF film with one side coated in gold acting as the ground plane. The positive array pattern of the transducer is formed on a copper clad polyimide film ("flex circuit"). The flex circuit and PVDF are bonded together, press fit into a spherical shape, and then back filled with epoxy. Transducer performance was characterized by measuring the pulse/echo response, two-way insertion loss, electrical cross talk, complex electrical impedance of each array element, and lateral -6-dB pulse/echo beamwidth.

II. MATERIALS AND METHODS

A. Fabrication

1) *Polyimide Array Patterns*: The circuit patterns were designed as positive images with a CAD software package (QuickCAD, Autodesk Inc., San Rafael, CA). The transducer we discuss here had a total aperture of 6 mm with five equal area rings separated by 100 μm kerf spacings [Fig. 1]. The electrical traces that permit access to each annulus and the spacing between the traces were also 100 μm . From the CAD file, a transparent film with the positive array image was generated by an offset print shop (Elite Graphics Co. Inc., New York, NY). This method of creating the positive image permitted us to achieve line widths and spacings of smaller than 100 μm .

The array pattern was formed on single sided, copper clad polyimide film (RFlex 1000L810, Rogers Corp., Chandler, AZ), a material commonly used to fabricate flex circuits. The polyimide film was 25- μm thick, the copper was 18- μm thick, and an adhesive layer bonding the copper to the polyimide was 20- μm thick. Before creating the array pattern, the polyimide was coated with a uniform thickness of positive photoresist (Injectorall, Bohemia, NY).

The fabrication of the copper array pattern utilized standard copper etching techniques. The positive array image was placed on top of the photoresist coated polyimide and exposed to ultraviolet (UV) light for 2-3 minutes in a UV fluorescent exposure unit (AmerGraph, Sparta, NJ). The polyimide was then transferred to a liquid developer, which removed the photoresist

that had been exposed to UV light. The developed film was then gently agitated in a ferric chloride bath until all the copper in the areas lacking photoresist had been etched away. The finished array pattern was viewed with a microscope to ensure that the line widths and spacings were uniform and of the correct size. After gently removing the remaining photoresist with steel wool, the pattern was tested for electrical continuity between the rings and copper contact pads. Test patterns were first utilized to ensure that we could achieve 100 μm spacing for both ring separations and line widths.

2) Press Fit Assembly: The final assembly of the transducer utilized a press fit technique similar to that used for single element PVDF [1], [26] and ceramic transducers [8], [10]. Figure 2 shows a schematic of the custom jig and material layers of the final assembly. The jig was constructed of aluminum and consisted of a base plate, a pressure plate to apply uniform pressure to the films as they were pressed, and a top plate to press in the ball bearing. The base plate had a central hole in which a Teflon tube was inserted. The Teflon tube ensured that the PVDF and polyimide films would not tear from the pinching at the transducer's edge during the press fit.

Assembly began by inserting the Teflon tube into the baseplate and then centering the array pattern over the Teflon tube with the copper side up. The inner diameter of the tube was larger than the active aperture of the array. A single drop of epoxy (Hysol RE2039, HD3561, Loctite Corp., Olean, NY) was placed onto the array pattern and a 4 cm by 4 cm section of PVDF membrane (Ktech Corp., Albuquerque, NM) was placed over the epoxy. The PVDF was 9 μm thick and had one side metallized with gold. The metallized side formed the ground plane of the transducer and faced upward. A Teflon ring was placed over the two films and then lightly clamped with the pressure plate. The pressure plate permitted the film layers to move slightly while also stretching during the press fit, thus minimizing crinkling of the films at the edge of the transducer.

A stainless steel ball bearing with an OD of 24 mm was then pressed into the films with the top plate and the plate was tightly secured. Next, the jig was turned over and the Teflon tube was filled with epoxy. The whole jig assembly was then placed into a vacuum chamber at ≈ 8 Torr. The degassing lasted as long as necessary to ensure that no bubbles were present on the backside of the polyimide (≈ 40 min).

After degassing, the jig was moved into a 40° C oven to reduce the epoxy cure time. When the epoxy had cured, the transducer was removed from the jig and separated from the Teflon tube. This left an epoxy plug with a smaller diameter curved array bonded to it. Excess material was trimmed away to leave just the electrical traces and their contact pads [Fig. 3]. To form a continuous ground plane, silver epoxy (EE129-4 Epoxy Technology, Billerica, MA) was used to join the conductive side of the PVDF to additional ground traces on the polyimide film.

In order to electronically access the array elements, a customized printed circuit board (PCB) was fabricated [Fig. 4]. The PCB had a 20-pin zero insertion force (ZIF) connector on one side (Hirose Electric, Simi Valley, CA) and miniature MMCX-BNC connectors on the other side (Amphenol, Wallingford, CT). BNC cables (RG-174 50 Ω) of 0.87 m length were connected to the MMCX connectors. An additional advantage of the PCB board was that surface mount inductors could be soldered directly onto the board to perform impedance matching. A mounting bracket made from aluminum rod held the transducer and PCB board. The polyimide film could then be wrapped around and inserted into the ZIF connector [Fig. 4].

B. Testing

1) Pulse/Echo: The transducers were first characterized by examining their pulse/echo response using a quartz-plate target positioned 12 mm from the transducer. The transducer was placed in a small container of degassed water with a 2.5-cm thick quartz plate at its bottom. The

transducer was then excited with a pulser/receiver (Panametrics 5900, Waltham, MA) while the return signal was digitized with a 1 GS/s, 8-bit digitizer (Acqiris DP110, Monroe, NY). The separation distance and tilt angle between the transducer and the quartz plate were adjusted to maximize the amplitude of the return echo.

2) *Two-Way Insertion Loss*: Two-way insertion loss measures the efficiency of a transducer by comparing the pulse/echo voltage response of a transducer to the voltage available at a 50 Ω load for the same excitation waveform. Insertion loss was measured utilizing a directional coupler (Minicircuits ZDC-10-1, Brooklyn, NY) [1] with the transducer on the coupler's in port, the excitation waveform on the coupler's out port, and the coupled port terminated into a digitizer (Acqiris DP110) with 50 Ω impedance.

To measure the pulse/echo voltage response, the transducer was excited with a quasi-continuous wave tone burst. The tone burst was 1 μ s in duration and originated from a function generator (Agilent 33250a, Palo Alto, CA) the output of which was gated via an RF switch (Minicircuits ZASWA-2-50DR). The transducer was submerged in degassed water with a thick quartz plate placed in its geometric focal plane and the echo signal from the front surface of the quartz reflector was windowed at a delay appropriate to the round trip water path distance. An automated LabVIEW program (National Instruments, Austin, TX) was then used to sweep through a frequency range in 1 MHz steps. At each frequency step, the peak-to-peak voltage V_{pp} of the return echo waveform was measured after the output of the coupler's coupled port passed through a limiter (Anritsu 1N50B, Richardson, TX) and was amplified by 32.5 dB (Miteq AU-1114, Hauppauge, NY). The voltage measurements were converted to dB and then corrected for the losses due to the quartz plate transmission coefficient (1.7 dB) and acoustic attenuation in water (2×10^{-4} dB/mm-MHz²) [8].

The transmit waveform, representing the voltage available to a 50 Ω load, was measured after creating an open circuit at the transducer by detaching the polyimide film from the ZIF connector on the PCB board. The open circuit at the ZIF connector causes full voltage reflection, with a zero time delay. The V_{pp} values were again measured in 1 MHz step at the coupler's coupled port, but without any additional amplification. Because all cabling was identical for both the pulse/echo and transmit measurements, the final frequency dependent insertion loss is calculated by subtracting the transmit results from the pulse/echo results.

3) *Complex Impedance*: After fabrication and the initial pulse/echo measurement, the complex impedance of each annulus was measured with a combination Network-Spectrum-Impedance Analyzer (HP4396A & HP43961A, Hewlett Packard, Palo Alto, CA). After compensating for the 0.87-m cable connecting the transducer to the analyzer, the capacitive reactive component of the impedance at 40 MHz was used to determine the appropriate series inductance needed to bring the reactance to zero. An appropriate surface mount inductor was selected and soldered directly onto the PCB board [Fig. 4]. The complex impedance was again measured to ensure that the reactance at the center frequency was in fact zero.

4) *Electrical Cross Talk*: Electrical cross talk between rings was measured by transmitting a 1 V_{pp} continuous wave signal on a single annulus and then measuring the voltages seen by the remaining annuli. The transmit voltage was measured with a high impedance 10X probe while the remaining annuli voltages were measured into 50 Ω terminations at the end of the 0.87 m BNC cables. The voltages were measured with a 4-channel digital oscilloscope (WaveRunner 6050, LeCroy, Chestnut Ridge, NY). The cross-talk measurements were made at several frequencies, including the center frequency of the transducer. The cross talk was expressed in dB as the ratio of the voltage on the receive annulus to the voltage on the transmit annulus. The transducer was not submerged in water for this measurement, as this did not change the results.

5) *Lateral Beamwidth*: The pulse/echo lateral beamwidth of each annulus was measured by scanning the transducer across a 25 μm wire target positioned at the geometric focus of the transducer. The scanning was performed with an automated XYZ motion system under LabVIEW control. The transducer was excited with a pulser/receiver (Panametrics 5900) and V_{pp} was recorded at 10 μm increments over a span of 0.8 mm. This method of measuring the lateral beam width approximates the case of a point scatterer and is valid as long as the wire diameter is smaller than the wavelength of sound [27].

III. RESULTS

The results shown here are for a 5-ring annular array with equal area elements and 100 μm kerf spacing between rings. The total transducer aperture was 6 mm and the radius of curvature was 12 mm. The outer diameter of the epoxy plug was 12.8 mm. The inner and outer radii of the annuli when projected onto a plane were 0, 1.22, 1.32, 1.8, 1.9, 2.26, 2.36, 2.65, 2.75 and 3.0 mm [Fig. 1]. The experimental data are compared to the results of a KLM model [28] (PiezoCAD, Sonic Concepts, Woodinville, WA) as a means to validate the performance of the transducer.

A. Unmatched Transducer

The pulse/echo time domain waveform acquired for Ring 1 (central annulus) is shown in Fig. 5(a). The other 4 rings, scaled relative to each other, showed similar time domain results with about a 50% reduction in amplitude compared to the center ring (Fig. 5(c)). The frequency domain signal for Ring 1 is shown in Fig. 5(b). The center frequency (f_c) is 39 MHz and the -6-dB fractional bandwidth (BW) is 61%. Both the time-domain and frequency-domain experimental results of Fig. 5 compare favorably to the predictions of the KLM model (dotted).

A summary of the power spectra for all five array elements is shown in Fig. 6, showing the shift towards lower sensitivities for the outer rings. The peak amplitude for Ring 1 is normalized to 0 dB. Table II summarizes the values for the peak amplitude, f_c , and BW for all five annuli. The table also shows the results for minimum insertion loss and the frequency at which it occurred. The insertion losses are consistent with what has been previously reported for PVDF based transducers [1].

B. Matched Transducer

Impedance measurements were made of each annulus in order to determine the most efficient electrical matching. The unmatched impedance of each element varied only slightly in value so that a single example is sufficient to demonstrate the approach and results [Fig.7(a)]. The impedances at 40 MHz for all of the rings are shown in Table I. The resistance for each element was $\approx 70 \Omega$ and for matching purposes the reactive component was taken to be $-j200 \Omega$. We chose to match the transducer capacitance with an inductor in series on the PCB. For simplicity, all of the array elements utilized the same matching inductance.

A value of 0.82 μH was calculated as the best matching at 40 MHz [Fig.7(b)]. In the ideal case the reactive component for each ring would be zero at 40 MHz. However, because we utilized only a single matching inductance, the frequency at which the matched reactance occurs varies somewhat for each ring [Tab. I]. Impedance plots found from the KLM model showed reactive values similar to the experimental results but did not predict the nearly 50% drop in resistance. The discrepancy likely occurs because the PCB and the flex circuit connection to the array add a complicated transmission line that was not fully accounted for in the KLM model.

With the impedance matching accomplished, we repeated the pulse/echo and insertion loss measurements. The time-domain pulse/echo signal and the KLM model prediction for Ring 1 are shown in Fig. 8(a) scaled relative to the unmatched cases (Fig. 5(a)). The corresponding

frequency domain signals are shown in Fig. 8(b), again scaled relative to the unmatched cases. The KLM model predicts a decrease in bandwidth and a downward shift in f_c , but less than what was observed experimentally. This may be due partly to the pulse/receiver and partly to not fully modeling the PCB and flex circuit.

The time domain pulse/echo for all five annuli are shown in Fig. 8(c) scaled relative to each other. As in the unmatched case, the amplitude drops by $\approx 50\%$ from Ring 1 to Ring 2 and then remains relatively constant for the remaining rings. The spectra for all five annuli are shown in Fig. 9. The peak amplitudes for Rings 1 to 5 increased by 12, 13, 12, 10 and 11 dB, respectively, relative to the unmatched cases. The values of the peak spectral amplitude, f_c , and BW for all five annuli are summarized in Tab. II. Comparing these values to the unmatched case, it can be seen that the increase in pulse/echo sensitivity has been achieved at the cost of reduced bandwidth and a lower center frequency.

The IL data for the matched cases are summarized in Tab. II. As in the unmatched case, the sensitivities of the annuli decrease somewhat for the outer rings. The matched case represents an improvement in insertion loss of 9, 8, 9, 5 and 7 dB over the unmatched case for Rings 1 to 5, respectively. The KLM model predicts a similar improvement in IL between the matched versus unmatched cases (≈ 10 dB) but with the absolute magnitudes of the IL lower than what was experimentally observed.

Cross talk was measured for only the matched case and the results are summarized in Table III. The table shows the cross talk for three excitation frequencies and three different transmit annuli. The cross talk was a minimum at the lowest frequency and increased with increasing frequency: ≈ -50 dB at 25 MHz, ≈ -42 dB at 40 MHz, ≈ -36 dB at 55 MHz. The electrical cross talk primarily arises from fringing effects at the edges of the copper array pattern and is most severe when there are sharp corners. The curvature of the rings is likely the main area of the copper pattern where fringing occurs rather than the parallel trace lines that lead out to the ZIF connector pads.

Lateral beamwidth was measured only for the matched case and Fig. 10 shows the results. The values of the -6 -dB beamwidths for Rings 1-5 are 230, 118, 80, 67, and 59 μm , respectively. As in the insertion loss and spectra data, the peak amplitude decreases sharply when moving from Ring 1 to Ring 2 and then the remaining rings are similar in value. Qualitatively, the decreasing beamwidth towards the outer rings may be understood in terms of the aperture. A larger aperture has a smaller beamwidth for a fixed focal length. Quantitatively, the beamwidth values agree favorably with numerical beam calculations based on the spatial impulse response method [29] using a typical pulse/echo response as the drive waveform in the model. The numerical beamwidth values for Rings 1-5 are 192, 104, 79, 66, and 58 μm , respectively. The numerical results vary somewhat depending on the drive waveform, but the trend of decreasing beamwidth towards the outer rings will always hold true. Beam profiles of each annulus were also recorded with a hydrophone and the results and trends were similar to those of the wire phantom.

IV. DISCUSSION

The performance of the PVDF array elements in terms of insertion loss, spectrum, and bandwidth, was similar to what has previously been reported for single element PVDF transducers [1]. Electrical impedance matching led to an improvement in two-way insertion loss, as predicted by the KLM model. One concern with this transducer design is that there are several layers between the PVDF and the epoxy backing plug: epoxy-copper-polyimide. These layers may potentially lead to a complicated internal reflection that could deteriorate the performance of the transducer. By studying the effects of the backing film thicknesses with our KLM model, we were able to determine how the layers affected performance. The copper

layer had the effect of making the PVDF a $\lambda/4$ resonator because of its high acoustic impedance (41.6 MRayls) relative to PVDF (4.2 MRayls) [1], [30]. The epoxy (3 MRayls) and polyimide (2.3 MRayls) layers primarily lowered the insertion loss and the BW. Internal reflections within the layers were not a problem because they were so thin and, at least for the polyimide and epoxy, their acoustic impedances were similar to that of PVDF.

The variation in sensitivities between the inner and outer rings was likely caused by two factors. First, the area of the outer rings was reduced slightly by the presence of the electrical traces (Fig. 1). As noted earlier, the array elements were designed to have equal areas for unbroken rings. However, the break in the rings only reduced the area by $\approx 3\%$ and does not explain the 6 dB drop in sensitivity observed in Table II.

Second, during the press fit, the ball bearing may not apply a uniform force across the whole surface area of the transducer. This problem may manifest itself in a slight defocusing of the transducer towards the outer rings and also in an increased thickness of the epoxy adhesion layer between the PVDF and the polyimide film towards the outer edge of the array. The thickness increase would both decrease the capacitance (make the reactance more negative) and increase the insertion loss as observed in Table I [30]. The KLM model showed a decreased sensitivity as the epoxy layer increases but did not capture the increased capacitance because the model assumes both sides of the PVDF have a conductive layer whereas our array design has the epoxy layer between the PVDF and one of its conductive layers.

We attempted to address the potential non-uniform epoxy layer problem by increasing the inner diameter of the press fit Teflon tube, thus increasing the distance between the active transducer area and the outer edge of the press fit. This helped to ensure that deviations in the epoxy adhesion layer thickness would not impact the active area of the transducer. The transducer tested here utilized this method with the larger Teflon tube and represented a considerable improvement over earlier prototypes that had a larger transducer aperture.

The electrical cross talk was measured at a fairly low drive voltage ($1 V_{pp}$) with the assumption that the values scale linearly with voltage. While we did not repeat the measurement at multiple drive voltages, we did look at the electrical cross talk when the annular array was driven with a high voltage, broadband pulse. Again we measured V_{pp} on the drive element and V_{pp} as seen by the other elements into a 50Ω termination. The results were most similar to the 55 MHz case in Tab. III. Based on these observations, the electrical cross talk does appear to increase with increasing voltage and is larger on transmit than on receive.

We were not able to observe any acoustic cross talk between elements. For this measurement, the transducer was submerged in water and one element was pulsed while the signals on the remaining elements were viewed with an oscilloscope. We then looked for signals showing a small delay relative to the excitation pulse. Acoustic cross-talk primarily arises from lateral coupling during the excitation pulse and is observed as a delayed pulse between array elements. The time delay of the pulse corresponds to the element separation distance and the shear velocity of the transducer material. For PVDF, the lateral coupling coefficient is very low ($k_{32} = 0.03$) compared to the thickness coupling coefficient ($k_t = 0.18$), and thus the lack of acoustic cross coupling is consistent with the material properties of PVDF.

V. CONCLUSION

We have demonstrated that PVDF based annular arrays can be constructed using a copper clad polyimide film to form the array electrode pattern. After impedance matching, the performance of the array elements was similar to what has been reported for single element PVDF transducers. The additional layers of material behind the PVDF film (epoxy-copper-polyimide) were found to not significantly hinder the transducer performance. This was due to their

thinness relative to λ and the close acoustic impedance match between the PVDF, epoxy, and polyimide. Electrical cross talk was on the order of -42 dB at 40 MHz and increased somewhat for high drive voltages. No significant acoustic cross coupling was observed between elements.

The advantage to the annular array demonstrated here is that its geometry is ideal for increasing the depth of field. To achieve a reasonable increase in the depth of field, the $F\#$ (focal length/OD) needs be greater than 2 [31]. An $F\#=2$ design with a total aperture of 6 mm permits an increase in the depth of field to ≈ 6 mm versus ≈ 1 mm for a single element transducer of the same geometry.

Our current efforts are to improve upon the present design and to develop a quasi-real time data acquisition system. With the new prototype, we plan to fully utilize the imaging capabilities of the annular array by acquiring data from individual transmit/receive annuli pairs and then implement digital synthetic aperture algorithms to reconstruct an image. For the testing, we will initially utilize a wire phantom to validate the array performance and then proceed to tissue models.

Figure 11 shows an example of data taken from the wire phantom. The phantom consists of seven $25\ \mu\text{m}$ wires spaced at 1 mm by 1 mm intervals. The transducer was scanned across the wire phantom with the center wire at the geometric focus. The image consists of 150 scan lines, found by averaging at each spatial location, spaced $25\ \mu\text{m}$ apart. Ring 1 was pulsed and the received signal on Ring 5 was digitized.

VI. Acknowledgements

The authors wish to thank George Keilman and Chris Vecchio for many useful discussions.

Biography

Jeffrey A. Ketterling (Member '02) was born in Seattle, WA, in 1970. He received the B.S. degree in electrical engineering from the University of Washington, Seattle, WA in 1994. He received the Ph.D. in mechanical engineering from Yale University, New Haven, CT, in 1999. His thesis focused on experimental studies of phase space stability in single bubble sonoluminescence. Since 1999 Dr. Ketterling has been a Member of the Research Staff at Riverside Research Institute, New York, NY. His research interests include high frequency arrays, transducer sound field modeling, and ultra sonic tissue characterization.

Orlando Aristizábal was born in Popayan, Colombia, on April 11, 1964. He received the B.S. degree in Physics in 1986 from City College of New York and the M.Phil. degree in Physics in 1993 from the Graduate Center of the City University of New York. During this time he studied the acoustomagnetic properties of Type I and Type II superconducting films. From 1993 to 1995 he was a visiting scholar at the University of Illinois in Urbana-Champaign where he studied the electrical properties of YBCO and other high temperature superconducting thin films. Since 1996 he has been a Research Scientist in the in vivo micro-imaging laboratory headed by Dr. Daniel Turnbull at the Skirball Institute of Biomolecular Medicine, New York University School of Medicine. His research interests are focused on the development and use of high frequency ultrasound imaging methods and their applications.

Daniel H. Turnbull (Member '92) was born in Niagara Falls, ON, Canada on April 11, 1955. He received the B.Sc. degree in Mathematics in 1978 from Brock University, St. Catharines, ON; the M.S. degree in Applied Mathematics in 1981 from the California Institute of Technology, Pasadena, CA; the M.A.Sc. degree in Mechanical Engineering in 1983 from the University of Toronto; and the Ph.D. degree in Medical Biophysics in 1991 from the University of Toronto, Toronto, ON, Canada.

He was a Systems Engineer at Imatron, Inc., a medical imaging company in San Francisco, CA from 1983 to 1986, and was a Medical Physicist at the Toronto-Sunnybrook Regional Cancer Center in Toronto, ON, Canada from 1991 to 1994. In 1994 he became an Assistant Professor in the Department of Medical Biophysics, University of Toronto, and soon after moved to New York University School of Medicine in New York, NY, where he was an Assistant Professor of Radiology and Pathology, and a member of the Structural Biology Program at the Skirball Institute of Biomolecular Medicine from 1994 to 2000. Since 2000, he has been an Associate Professor of Radiology and Pathology, and a member of the Structural Biology Program at the Skirball Institute of Biomolecular Medicine, New York University School of Medicine in New York, NY. For the past decade, his research interests have been broadly focused on the use of ultrasound and magnetic resonance micro-imaging in biology.

Frederic L. Lizzi (S62-M71) was born in Brooklyn, NY, in 1942. He received the B.E.E. degree from Manhattan College, Bronx, NY, in 1963 and the M.S. and Eng.Sc.D. degrees from Columbia University, New York, NY, in 1965 and 1971, respectively.

He is currently the Research Director of the Biomedical Engineering Laboratories at Riverside Research Institute, New York, NY, where he has been pursuing biomedical research in therapeutic and diagnostic ultrasound since the 1960s. He serves as principal investigator for a number of research programs supported by the National Institutes of Health that deal with ultrasonic imaging, tissue characterization, and therapeutic ultrasound. He is an adjunct professor at Cornell University and Columbia at University.

Dr. Lizzi is a Fellow of the American Institute of Ultrasound in Medicine (AIUM) and the Acoustical Society of America. He also is a member of the Advisory Editorial Board of Ultrasound in Medicine and Biology and a member of the board of the International Society for Therapeutic Ultrasound. Dr. Lizzi has served as a member of the Board of Governors of the AIUM and Chairman of the AIUM Bioeffects Committee. He has received the Mayneord Lecturer Award from the British Institute of Radiology, the AIUM William J. Fry Memorial Award, the AIUM Joseph Holmes Pioneer Award, and the Pioneer Award from the World Federation of Ultrasound in Medicine.

REFERENCES

1. Sherar MD, Foster FS. The design and fabrication of high-frequency poly(vinylidene fluoride) transducers. *Ultrason. Imaging* 1989;11:75–94. [PubMed: 2734975]
2. Foster FS, Harasiewicz KA, Sherar MD. A history of medical and biological imaging with polyvinylidene fluoride (PVDF) transducers. *IEEE Trans. Ultrason. Ferroelect. Freq. Contr* 2000;47:1363–1371.
3. Lockwood GR, Hunt JW, Foster FS. The design of protection circuitry for high-frequency ultrasound imaging systems. *IEEE Trans. Ultrason. Ferroelect. Freq. Contr* 1991;38:48–55.
4. Lockwood GR, Foster FS. Modeling and optimization of high-frequency ultrasound transducers. *IEEE Trans. Ultrason. Ferroelect. Freq. Contr* 1994;41:225–230.
5. Lockwood GR, Hazard CR. Miniature polymer transducers for high frequency medical imaging. *Proc. SPIE Med. Imag* 1998;3341:228–236.
6. Talman JR, Garverick SL, Morton CE, Lockwood GR. Unit-delay focusing architecture and integrated-circuit implementation for high-frequency ultrasound. *IEEE Trans. Ultrason. Ferroelect. Freq. Contr* 2003;50:1455–1463.
7. Brown JA, Lockwood GR. A low-cost, high-performance pulse generator for ultrasound imaging. *IEEE Trans. Ultrason. Ferroelect. Freq. Contr* 2002;49:848–851.
8. Lockwood GR, Turnbull DH, Foster FS. Fabrication of high frequency spherically shaped ceramic transducers. *IEEE Trans. Ultrason. Ferroelect. Freq. Contr* 1994;41:231–235.
9. Aristizábal O, Turnbull DH. 44-MHz LiNbO₃ transducers for UBM-guided Doppler ultrasound. *IEEE Trans. Ultrason. Ferroelect. Freq. Contr* 2003;50:623–630.

10. Cannata JM, Ritter TA, Chen WH, Silverman RH, Shung KK. Design of efficient, broadband single-element (20-80 MHz) ultrasonic transducers for medical imaging applications. *IEEE Trans. Ultrason. Ferroelect. Freq. Contr* 2003;50:1548–1557.
11. Lockwood GR, Turnbull DH, Christopher DA, Foster FS. Beyond 30 MHz - Applications of high-frequency ultrasound imaging. *IEEE Eng. Med. Biol. Mag* 1996;15:60–71.
12. Silverman RH, Rondeau MJ, Lizzi FL, Coleman DJ. Three-dimensional high-frequency ultrasonic parameter imaging of anterior segment pathology. *Ophthalmology* 1995;102:837–843. [PubMed: 7777285]
13. Turnbull DH, Starkoski BG, Harasiewicz KA, Semple JL, From L, Gupta AK, Sauder DN, Foster FS. 40-100 MHz B-scan ultrasound backscatter microscope for skin imaging. *Ultrasound Med. Biol* 1995;21:79–88. [PubMed: 7754581]
14. Harland CC, Kale SG, Jackson P, Mortimer PS, Bamber JC. Differentiation of common benign pigmented skin lesions from melanoma by high-resolution ultrasound. *Br. J. Dermatol* 2000;143:281–289. [PubMed: 10951134]
15. Vogt M, Knuttel A, Hoffman K, Altmeyer P, Ermert H. Comparison of high frequency ultrasound and optical coherence tomography as modalities for high resolution and non invasive skin imaging. *Biomedizinische Technik* 2003;48:116–121. [PubMed: 12838793]
16. Foster FS, Pavlin CJ, Harasiewicz KA, Christopher DA, Turnbull DH. Advances in ultrasound biomicroscopy. *Ultrasound Med. Biol* 2000;26:1–27. [PubMed: 10687788]
17. Turnbull DH, Foster FS. Ultrasound biomicroscopy in developmental biology. *Trends Biotechnol* 2002;20:S29–S33.
18. Phoon CKL, Turnbull DH. Ultrasound biomicroscopy-Doppler in mouse cardiovascular development. *Physiol. Genomics* 2003;14:3–15. [PubMed: 12824473]
19. Oralkan O, Ergun AS, Johnson JA, Karaman M, Demirci U, Kaviani K, Lee TH, Khuri-Yakub BT. Capacitive micromachined ultrasonic transducers: Next-generation arrays for acoustic imaging? *IEEE Trans. Ultrason. Ferroelect. Freq. Contr* 2002;49:1596–1610.
20. Fleischman A, Modi R, Nair A, Talman J, Lockwood G, Roy S. Miniature high frequency focused ultrasonic transducers for minimally invasive imaging procedures. *Sens. and Actuators, A* 2003;103:76–82.
21. Ritter TA, Shrout TR, Tutwiler R, Shung KK. A 30-MHz piezo-composite ultrasound array for medical imaging applications. *IEEE Trans. Ultrason. Ferroelect. Freq. Contr* 2002;49:217–230.
22. Cannata, J.; Shrout, T.; Shung, K. Proc. IEEE 13th Int. Symp. Appl. Ferroelect. Nara; Japan: 2002. A 35 MHz linear ultrasonic array for medical imaging; p. 343-346.
23. Snook, K.; Shrout, T.; Shung, KK. Proc. IEEE 13th Int. Symp. Appl. Ferroelect. Nara; Japan: 2002. Design of a 50 MHz annular array using fine-grain lead titanate; p. 351-354.
24. Morton C, Lockwood G. Design of a 40 MHz annular array. *Proc. IEEE Ultrason. Symp* 2001;2:1135–1138.
25. Brown JA, Démoré CEM, Lockwood GR. Design and fabrication of annular arrays for high-frequency ultrasound. *IEEE Trans. Sonics Ultrason* 2004;51:1010–1017.
26. Alves CH, Shook K, Ritter T, Shung KK. High frequency single element and annular array transducers incorporating PVDF. *Proc. SPIE Med. Imag* 2000;3982:116–121.
27. Raum K, Obrien WD. Pulse-echo field distribution measurement technique for high-frequency ultrasound sources. *IEEE Trans. Sonics Ultrason* 1997;44:810–815.
28. Leedom D, Krimholtz R, Matthaei GL. Equivalent circuits for transducers having arbitrary even- or odd-symmetry piezoelectric excitation. *IEEE Trans. Sonics Ultrason* 1971;18:128–141.
29. Arditi M, Foster FS, Hunt JW. Transient fields of concave annular arrays. *Ultrason. Imaging* 1981;3:37–61. [PubMed: 7195094]
30. Brown LF. Design considerations for piezoelectric polymer ultrasound transducers. *IEEE Trans. Ultrason. Ferroelect. Freq. Contr* 2000;47:1377–1396.
31. Arditi M, Taylor WB, Foster FS, Hunt JW. An annular array system for high-resolution breast echography. *Ultrasonic Imaging* 1982;4:1–31. [PubMed: 7199769]



Fig. 1.

Example of positive array image. The kerf spacings between the annuli are $100\ \mu\text{m}$. The traces to the right that permit electrical access to each ring and the spacings between them are also $100\ \mu\text{m}$. The central annulus is Ring 1 and the outer annulus is Ring 5. Note that the scale is not uniform.

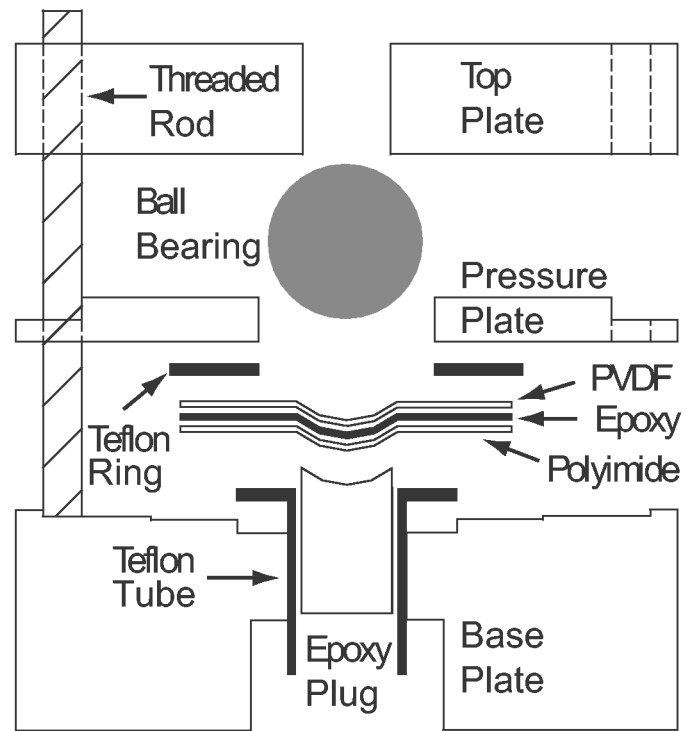


Fig. 2. Press fit jig. The pressure plate and top plate are clamped down with screws on the threaded rod.

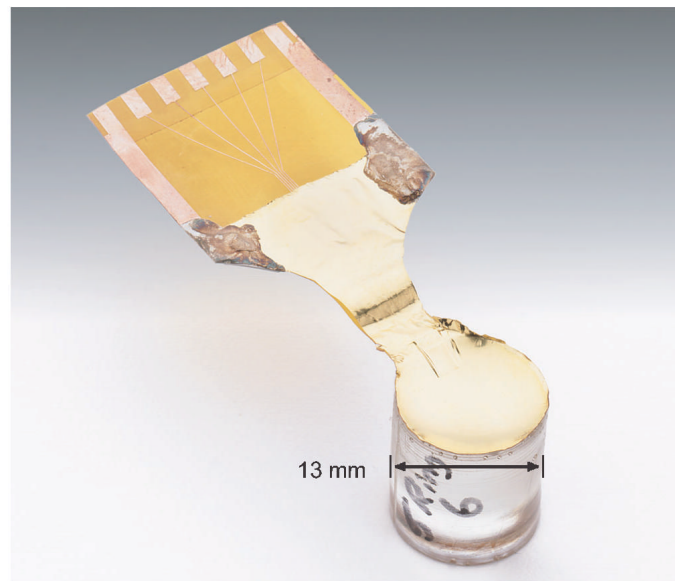


Fig. 3. Fully fabricated transducer. The active array is on top of the epoxy plug. The electrical traces at the top of the image are inserted into the ZIF connector.

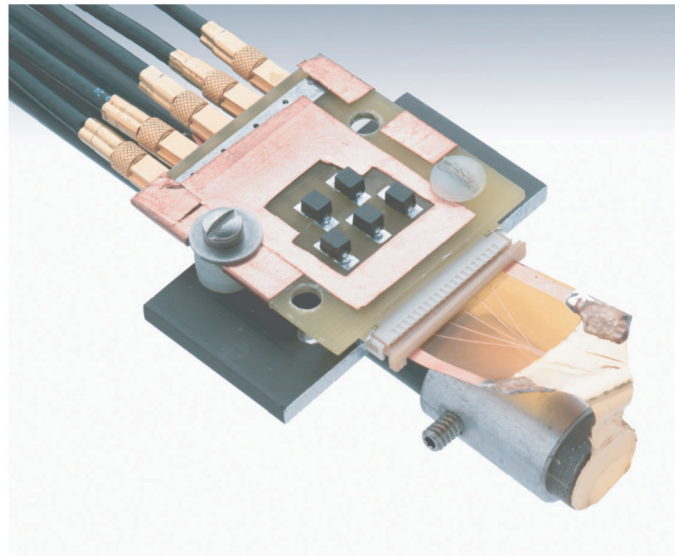


Fig. 4. PCB that links the traces on the polyimide to MMCX-BNC connectors. The polyimide wraps around and is inserted into the ZIF connector. This example also shows surface mount inductors soldered in series onto the PCB. The PCB is wrapped with copper tape for electrical shielding.



Fig. 5. Comparison of KLM model results (dotted) to experimental measurements (solid) for Ring 1 with no electrical matching. The results show the pulse/echo response in (a) the time domain, (b) the frequency domain, and (c) the time domain signal for all five array elements.



Fig. 6. Quartz plate pulse/echo power spectrum for all five rings of the annular array with no electrical matching. The values are normalized to the peak value of Ring 1.

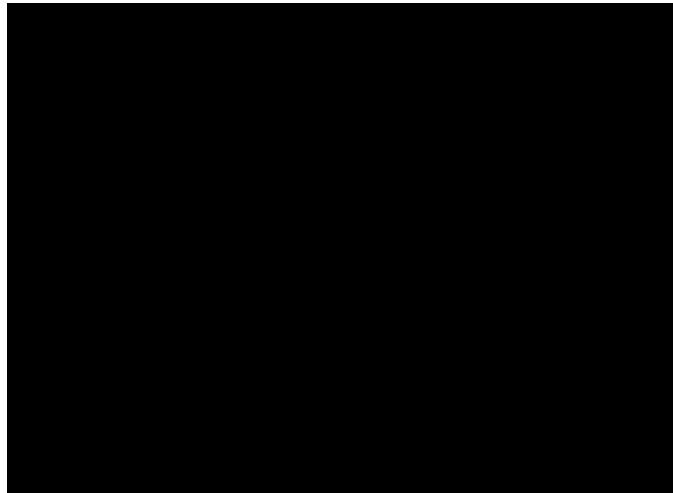


Fig. 7. Impedance of Ring 4 for the (a) unmatched and (b) matched case. The matched case has a 0.82 μH inductor soldered on the PCB with the result of reducing the reactance (dashed) to near zero at 40 MHz.

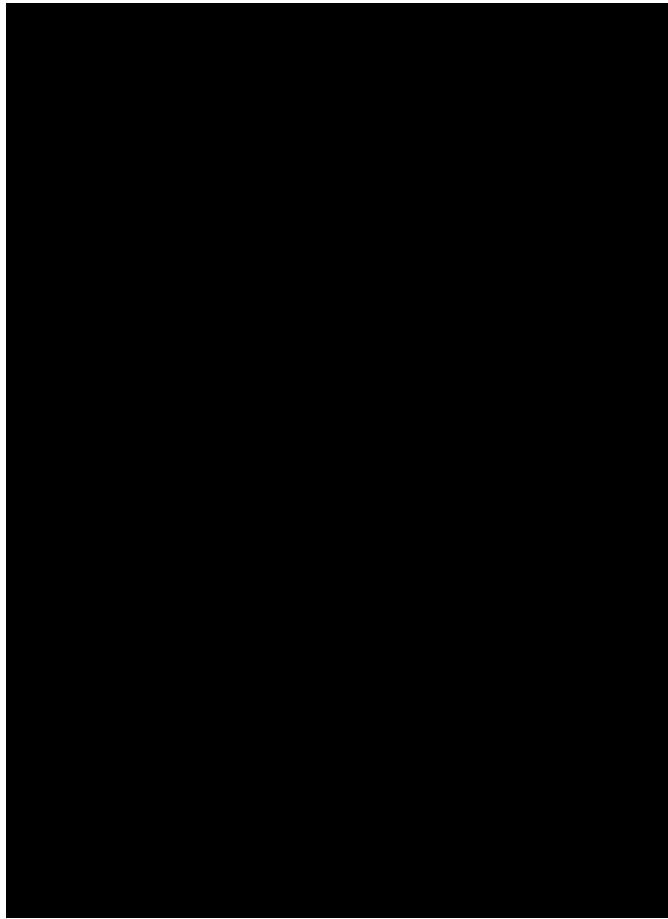


Fig. 8. Comparison of KLM model results (dotted) to experimental measurements (solid) for Ring 1 with electrical matching. The results show the pulse/echo response in (a) the time domain, (b) the frequency domain, and (c) the time domain signal for all five array elements.

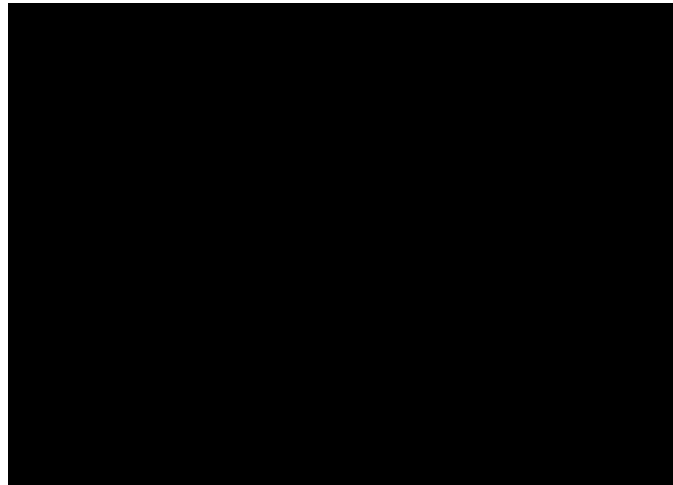


Fig. 9. Quartz plate pulse/echo power spectrum for all five rings of the annular array with a $0.82 \mu\text{H}$ inductor in series on the PCB. Amplitudes are relative to Ring 1 of the unmatched case.



Fig. 10. Pulse/echo lateral beamwidth for each annulus taken by scanning across a 25 μm wire target.

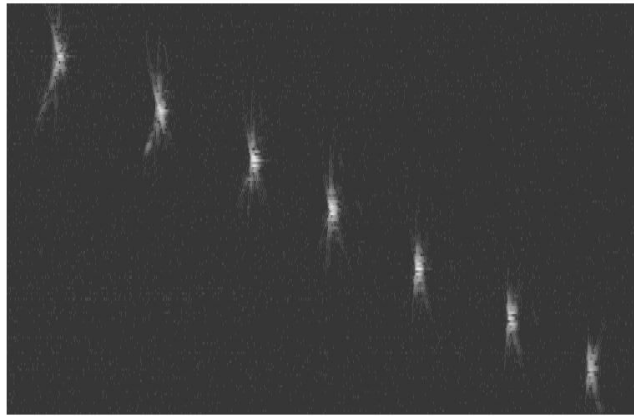


Fig. 11. B-mode image of a wire phantom found by mechanically scanning the annular array across the phantom. The image dimensions are ≈ 7 mm by 7 mm and the array was located to the left of the image. The data has been log compressed to provide better contrast. The dynamic range of the image is 64 dB.

TABLE I

ARRAY ELEMENT IMPEDANCES

Ring	f (MHz)	Unmatched Ω	f (MHz)	Matched Ω
1	40	$63-j187$	37	$38-j1.8$
2	40	$80-j219$	38	$36-j$
3	40	$68-j201$	39	$35+j2$
4	40	$70-j200$	37	$34+j1.5$
5	40	$68-j196$	38	$36+j0.5$

TABLE II

SUMMARY OF TRANSDUCER PERFORMANCE

Ring	f_c (MHz)	BW_{6dB} (%)	Unmatched			f_c (MHz)	BW_{6dB} (%)	Matched		
			dB_{max}	f_{IL} (MHz)	IL (dB)			dB_{max}	f_{IL} (MHz)	IL (dB)
1	39	61	0	50	-35	35	36	12	38	-28
2	38	54	-6	45	-45	36	31	7	38	-33
3	39	53	-6	46	-44	36	33	6	40	-35
4	41	52	-6	50	-43	36	35	4	42	-38
5	42	57	-7	50	-43	37	39	4	41	-36

TABLE IIIELECTRICAL CROSS TALK FOR MATCHED TRANSDUCER¹

Ring	25 MHz			40 MHz			55 MHz		
1	-55	-	-50	-46	-	-41	-39	-	-35
2	-53	-42	-38	-46	-39	-35	-37	-35	-35
3	-53	-51	-	-45	-43	-	-36	-35	-
4	-42	-51	-52	-40	-44	-40	-35	-36	-34
5	-	-55	-51	-	-46	-42	-	-36	-35

¹All values expressed in dB. A (-) indicates the excitation ring.